Available online at www.sciencedirect.com
SCIENCE DIRECT®
International Journal of Hydrogen Energy 30 (2005) 1569–1581
International Journal of HYDROGEN ENERGY
www.elsevier.com/locate/ijhydene

Experiments on a metal hydride-based hydrogen storage device

P. Muthukumar, M. Prakash Maiya, S. Srinivasa Murthy*

Refrigeration and Air Conditioning Laboratory, Department of Mechanical Engineering, Indian Institute of Technology, Madras, Chennai 600036, India

Available online 26 January 2005

Abstract

Metal hydride-based hydrogen storage devices are tested using AB_5 alloys, namely $MmNi_{4.6}Fe_{0.4}$ and $MmNi_{4.6}Al_{0.4}$. Performance studies are carried out by varying the supply pressure, absorption temperature and overall heat transfer coefficient. At any given absorption temperature, hydrogen absorption rate and storage capacity are found to increase with supply pressure for both the alloys. At a supply pressure of 35 bar and a cold fluid temperature of 15 °C, $MmNi_{4.6}Fe_{0.4}$ alloy stored about 1.6 wt%, while $MmNi_{4.6}Al_{0.4}$ stored 1.3 wt%. Cold fluid temperature is found to have a significant effect on hydrogen storage capacity at lower supply pressures. The overall heat transfer coefficient has a negligible influence on the hydrogen storage capacities of both the alloys. However, higher values of overall heat transfer coefficients yield better rates of absorption and desorption.

Keywords: Hydrogen storage; Metal hydride

1. Introduction

It is well established that many inter-metallic alloys are capable of absorbing and releasing hydrogen without compromising their own structure. Manipulation of absorption temperature or supply pressure can influence the storage capacities and absorption rates. Similarly, desorption rates can also be controlled by varying the desorption temperatures.

Many investigators have synthesized a variety of alloys and have studied their hydrogen absorption and desorption characteristics. Sinha and Wallace [1] studied the characteristics of $Zr_{0.7}Ti_{0.3}Mn_2Fe_{0.8}$ and found that the alloy has fast reaction kinetics (50% hydrogen was absorbed in 3–4 s while 90% hydrogen was absorbed in only 40 s) and also that it possessed about 1.5 wt% storage capacity. Later, they [2] studied the hydrogen absorption characteristics of $TiMn_{1.5}$ and $Zr_{1-x}TiMn_yFe_z$ (substoichiometric in zirconium in the range $0 < x < 0.3$ keeping $y + z = 1$), which were found to yield large storage capacity, favorable equilibrium pressure and rapid sorption kinetics. Sinha et al. [3] also studied the hydrogen storage characteristics of $Zr_{0.8}Ti_{0.2}MnCr_{1.25}$, $ZrMnFeT_x$ (T = Cr, Ni, Co; $0 < x < 0.4$) and $ZrCrFe_{1+x}$ ($0 < x < 0.5$) in the temperature and pressure ranges of 23–150 °C and 0.1–50 atm, respectively. $ZrCrFe_{1.5}$ was found to have a moderate equilibrium pressure of about 2 bar at 296 K and nearly 1.45 wt% storage capacity. Topler and Feucht [4] tested the kinetics of $Ti_{0.98}Zr_{0.02}Cr_{0.05}V_{0.43}Fe_{0.09}Mn_{1.5}$ for automobile applications. Hagstrom et al. [5] studied the applicability of six hydrogen absorbing alloys, namely $MmNi_{4.5}Mn_{0.45}Zr_{0.05}$, $Zr_{0.7}Ti_{0.3}MnFe$, $La_{1-x}Nd_xNi_5$, LmNi(1), Hydroalloy C15 and $Zr(Fe_{0.75}Cr_{0.25})_2$ at temperatures of 10–50 °C and pressures of 1–20 bar. They found that large hysteresis effect and sloping *P–C–T* plateau are the serious problems associated with $MmNi_{4.5}Mn_{0.45}Zr_{0.05}$, $Zr_{0.7}Ti_{0.3}MnFe$ and LmNi(1) alloys. Even though $Zr(Fe_{0.75}Cr_{0.25})_2$ suffered both from hysteresis and sloping *P–C–T* plateau, it

* Corresponding author. Tel.: +91 44 2257 8524; fax: +91 44 2257 0545.
E-mail address: ssmurthy@iitm.ac.in (S.S Murthy).

0360-3199/$30.00
doi:10.1016/j.ijhydene.2004.12.007

Nomenclature

m_a	mass of alloy, kg
P	pressure, bar
T	temperature, °C
U	overall heat transfer coefficient, $W/m^2\,K$

Subscripts

a	absorption
c	cold fluid
d	desorption
f	heat transfer fluid
h	hot fluid
s	supply
1,2,3,4,5	sensor locations (Fig. 2)

was recommended as a hydrogen storage material for fuel cell applications. Storage capacities of the tested alloys were about 1.4–1.5 wt%. Singh et al. [6] investigated the hydrogen sorption characteristics of $FeTi_{1+x}$ + 4.5%Mm ($x = 0.3$, 0.4 and 0.5) at room temperature and at 100 °C. The maximum storage capacity of about 1.71 wt%, which corresponded to $x = 0.3$, was observed at 20 bar supply pressure and at room temperature. Hydrogen storage capacity was found to increase up to about 1.9 wt% at 100 °C. Davidson and Srivastava [7] prepared the Mm, Ti-substituted $Zr_{1-2x}Mm_xTi_xFe_{1.4}Cr_{0.6}$ ($x = 0$, 0.05, 0.1 and 0.2) Laves phase alloys, which revealed a high hydrogen storage capacity of about 1.75 wt%. The optimized sample corresponded to the composition at $x = 0.05$. The results confirmed the conjecture that the Mm and Ti substitution increased both the storage capacity and kinetics. Du [8] reported the hydrogen storage properties of $Zr_{0.8}Ti_{0.2}(Ni_{0.6}Mn_{0.3-x}V_{0.1+x}Cr_{0.05})_2$ ($x = 0.0$, 0.05, 0.15 and 0.2) alloys. The effects of substitution of Mn by V atoms on phase structure and hydrogen storage properties were studied. Sitaram et al. [9] studied the hydrogen storage properties and the thermodynamics of hydrogen absorption in $Zr_{0.9}Ho_{0.1}MnFe_{0.5}Co_{0.5}$ and $Zr_{0.9}Ho_{0.1}MnFe_{0.5}Ni_{0.5}$ alloys. Singh et al. [10] synthesized $MmNi_{5-x}Fe_x$ alloys ($x = 0.05$, 0.1, 0.3 and 0.5) and found that substitutions up to 0.1 concentration of Fe lead to enhancement in storage capacity. Thus, the material $MmNi_{4.9}Fe_{0.1}$ yielded a storage capacity of 1.66 wt%.

While a large number of works have been reported on the steady-state *P–C–T* characteristics of small alloy samples under controlled laboratory conditions, their performance in larger storage systems under dynamic operating condition has not been studied. In practice, heat and mass transfer within the hydride bed play an important role. In the present study, a hydrogen storage device using two mischmetal-based alloys is tested for its performance at various supply pressures, cold fluid temperatures and overall heat transfer coefficients.

2. Experimental setup

Alloys for hydrogen storage application should have high hydrogen storage capacity, low plateau pressure and fast reaction kinetics. In addition, importance should also be given to flat plateau, low hysteresis, easy activation and availability at low cost. With the aid of a basic screening procedure devised by the authors [11] and considering availability and practical constraints, mischmetal-based alloys $MmNi_{4.6}Fe_{0.4}$ and $MmNi_{4.6}Al_{0.4}$ are selected for the present study.

The metal hydride reactor considered here is of annular cylindrical configuration as shown in Fig. 1. Heat transfer fluid flows spirally through the space between the reactor (inner concentric tube) and heat transfer fluid jacket (outer concentric tube) while the alloy fills the space between the inner tube and the filter. The reactor is made of a seamless stainless steel (SS-316) tube of wall thickness of 3 mm and the filter is of sintered SS-316 of 2 μm pore size. Eight radial copper fins 1 mm thick are used to enhance the effective thermal conductivity of the hydride bed. One end of the reactor is closed with the brazed assembly of four-grounded metal-sheathed "K" type thermocouples (sensitivity 0.1 °C) and the other end of the reactor is flanged. Other instrumentation and sensors are shown in Fig. 2. Piezoresistive-type pressure transducers of range 0–100 bar (sensitivity 0.01 bar) are used for measuring the reaction pressure (P_1) and the supply pressure (P_2). A coriolis mass flow meter (sensitivity 0.001 g) is used for measuring the hydrogen flow rate, total flow and temperature of the hydrogen gas. High-pressure packless type bellow valves are used in the gas line for controlling/diverting the gas flow. Two constant temperature baths (accuracy ±0.1 °C) are used for supplying hot and cold fluids at flow rates ranging from 1 to 3.5 l/min. The overall heat transfer coefficient is varied from 750 to 1250 $W/m^2\,K$ by varying the heat transfer fluid flow rates from 1 to 3.5 l/min.

Activation of the two Mm-based alloys is carried out at high pressure and at nearly room temperature. Fig. 3 shows the progressive activation of the alloys at 27 °C and at 80 bar pressure. Before letting hydrogen gas in to the reactor, it is evacuated down to about 10^{-3} mbar. Then the whole system was flushed 3 times using hydrogen gas to remove any other trace gases. Then hydrogen at 80 bar pressure was allowed to the reactor and the mass flow meter reading was monitored. During the first cycle of operation, hydrogen absorption of about 0.5 wt% was observed in 30 min. Then the reactor is heated up to 60 °C and the hydrogen was

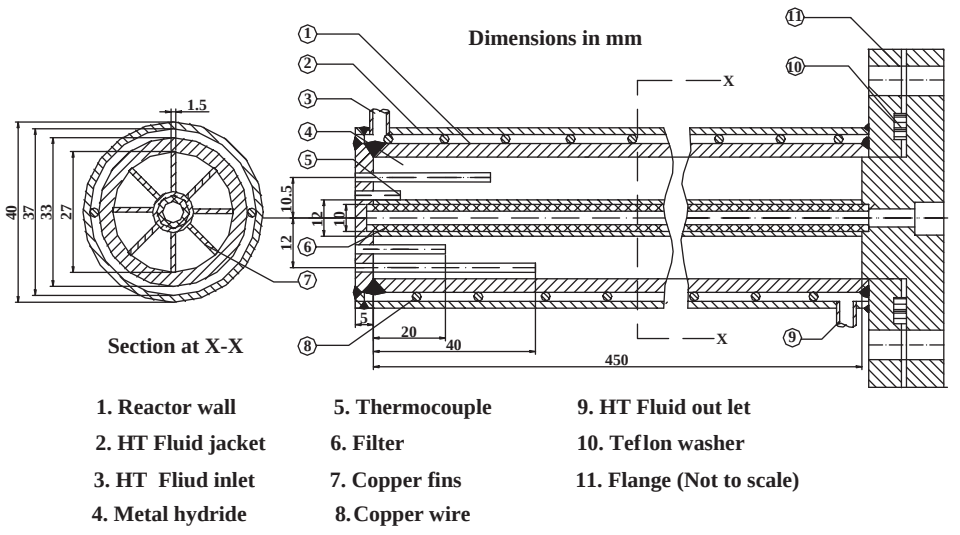

Fig. 1. Schematic of the cylindrical reactor.

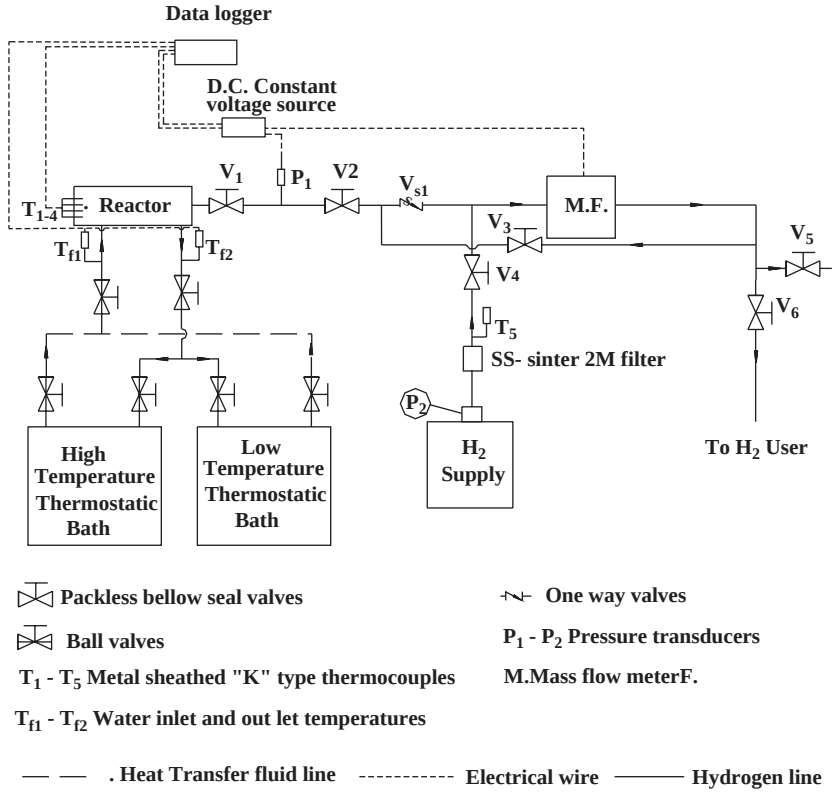

Fig. 2. Test setup for hydrogen storage device with mischmetal-based hydrides.

completely desorbed. This was repeated till the maximum storage capacities of 1.65 and 1.43 wt% were attained for $MmNi_{4.6}Fe_{0.4}$, and $MmNi_{4.6}Al_{0.4}$ alloys, respectively, in eleven cycles as seen in Fig. 3.

At the start of each experiment, efforts are made to have the same initial condition of the reactor. First, the reactor is evacuated down to 10^{-3} mbar. Valves V_1 to V_4 are opened and hydrogen (25 bar for $MmNi_{4.6}Fe_{0.4}$ and 15 bar

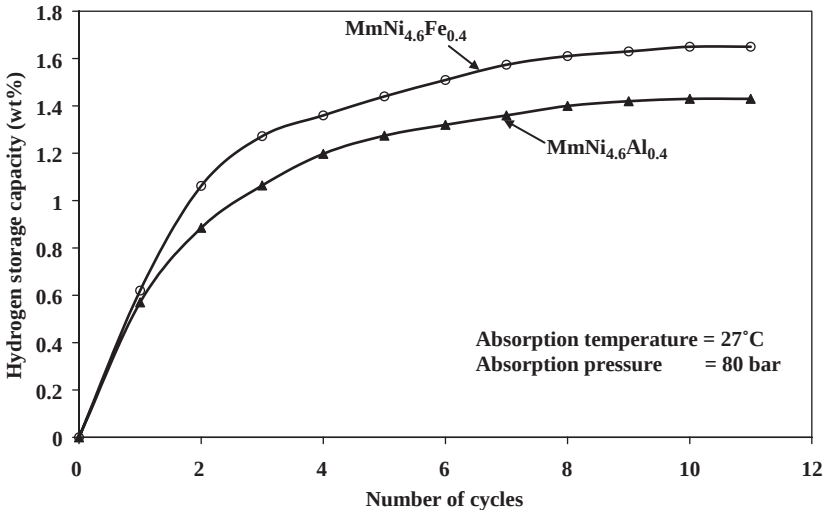

Fig. 3. Activation of hydrogen storage alloys.

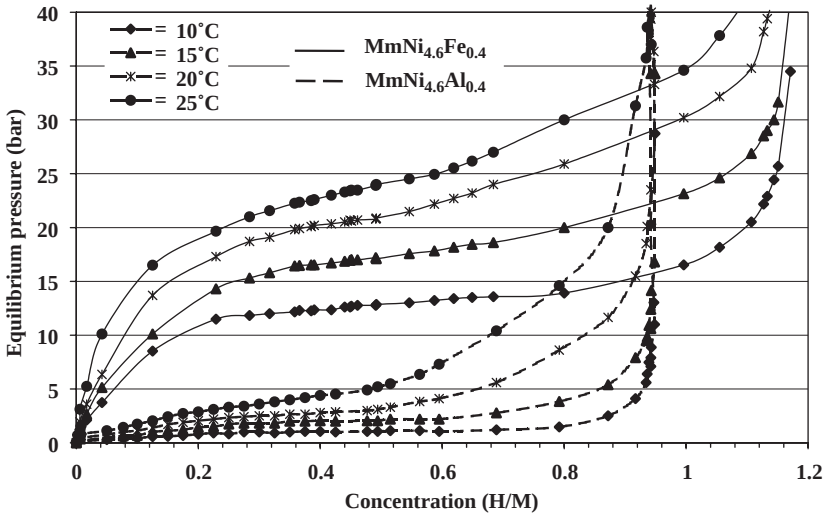

Fig. 4. *P–C–T* characteristics of the two mischmetal-based alloys.

for $MmNi_{4.6}Al_{0.4}$) is allowed to flow into the reactor. The alloy absorbs hydrogen by releasing heat of absorption, which is removed by circulating cold fluid at 25 °C. When the whole bed attains a uniform temperature of 25 °C and absorption has ceased, valves V_1 to V_4 are closed. Then the bed is heated to certain hot fluid temperature (50 °C for $MmNi_{4.6}Fe_{0.4}$ and 60 °C for $MmNi_{4.6}Al_{0.4}$) and then hydrogen is desorbed by opening valves V_1, V_2 and V_6, through a pressure relief valve V_{s1}. It is observed that the desorbed quantity is always less by about 3–4% than that of the absorbed quantity. Based on the difference, the initial concentration of the bed is calculated for both alloys and the initial concentration varied between 0.04 and 0.07.

At the start of the storage cycle, the bed is cooled by circulating the cold fluid. Later, valves V_1 to V_4 are opened, and absorption of hydrogen is continued till the supply pressure becomes equal to the hydride equilibrium pressure, which completes the absorption process. During this period, temperatures T_1 to T_5, T_{f1} and T_{f2}, pressures $P_1$and P_2, and mass flow rate and total flow of hydrogen are recorded for every 0.1 s. Heat of absorption is rejected to the cold fluid. Valves V_1 to V_4 are closed and then the reactor is brought to the ambient temperature. The bed is heated to the desired desorption temperature causing the pressure of the hydride bed to increase to the equilibrium pressure. Valves V_1, V_2 and V_6 are opened and the

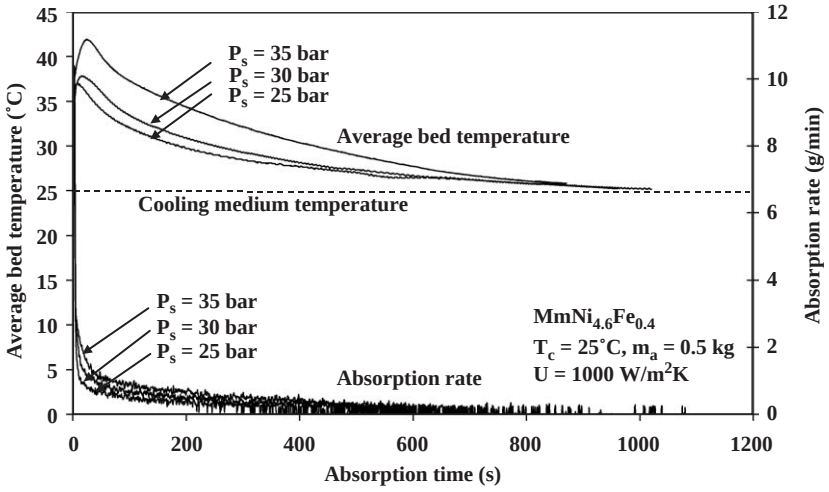

Fig. 5. Effect of supply pressure on average bed temperature and hydrogen absorption rate for $MmNi_{4.6}Fe_{0.4}$.

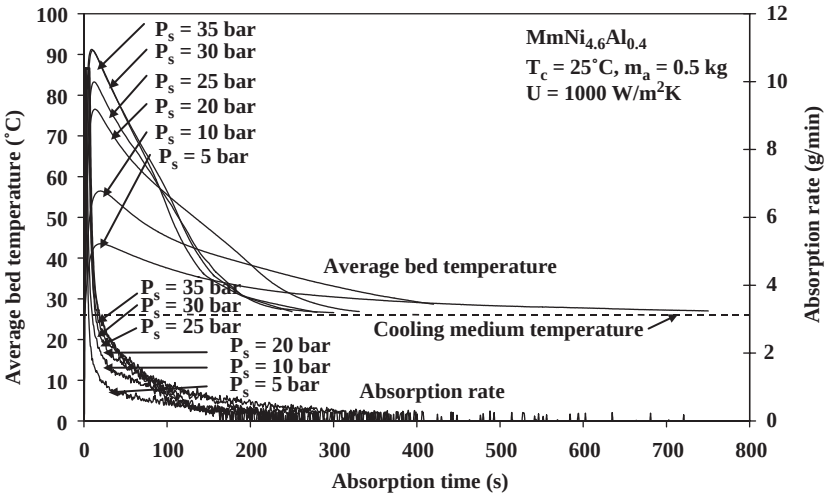

Fig. 6. Effect of supply pressure on average bed temperature and hydrogen absorption rate for $MmNi_{4.6}Al_{0.4}$.

desorbed hydrogen is directed to the user at 1 bar. During this period, the measurements made during the absorption process are repeated. Using a pressure-reducing valve, the supply pressure is varied from 5 to 40 bar for subsequent tests.

3. Results and discussion

The performance of a hydrogen storage device is mainly denoted by the hydrogen storage capacity, and the rates of absorption and desorption. Hence, the foregoing discussion is based on these parameters.

3.1. Effects of supply pressure

The reactor is allowed to absorb hydrogen at different supply pressures maintaining constant temperature of cold fluid at 25 °C. The flow rate of cold fluid is maintained to match the overall heat transfer coefficient $U = 1000\,W/m^2\,K$ (flow rate = 2.2 l/ min).

Fig. 4 shows the experimental *P–C–T* characteristics of $MmNi_{4.6}Fe_{0.4}$ and $MmNi_{4.6}Al_{0.4}$. At any given absorption temperature, the hydride concentrations at different pressures for both alloys are calculated based on the amount of hydrogen absorbed. It should be noted that at the end of the absorption process, the hydride equilibrium pressure

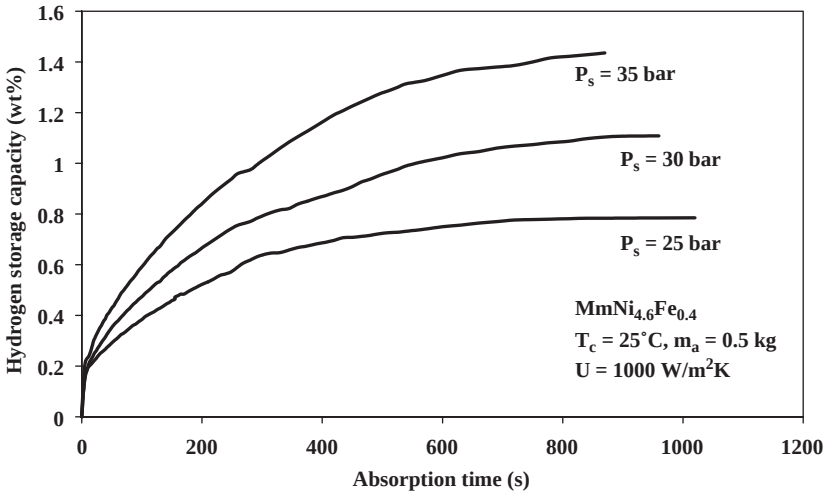

Fig. 7. Effect of supply pressure on hydrogen storage capacity for $MmNi_{4.6}Fe_{0.4}$.

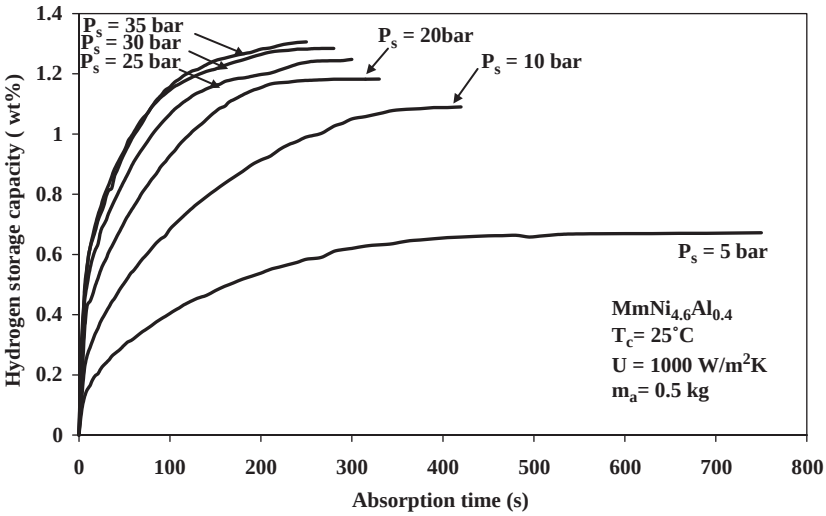

Fig. 8. Effect of supply pressure on hydrogen storage capacity for $MmNi_{4.6}Al_{0.4}$.

becomes equal to that of the supply pressure. Hence, the *P–C* curve is obtained from the values of supply pressures and the corresponding calculated hydride concentrations. The procedure is repeated for different absorption temperatures. It is observed that for any given temperature, $MmNi_{4.6}Fe_{0.4}$ has higher equilibrium pressure and correspondingly a larger slope than that of $MmNi_{4.6}Al_{0.4}$. Due to this, the former demands a higher supply pressure of above 35 bar while the latter requires above 30 bar for completing the absorption at 25 °C.

Figs. 5 and 6 show the variations of absorption rate and average bed temperature for $MmNi_{4.6}Fe_{0.4}$ and $MmNi_{4.6}Al_{0.4}$, respectively. It is observed that for a given supply pressure, the absorption rate instantaneously reaches a peak initially and decreases gradually towards zero at the end of the absorption process. This is due to the fact that at the start of the absorption process, the driving potential for mass transfer (difference between the hydrogen supply pressure and the hydride equilibrium pressure) is high, leading to fast reaction. As time progresses, hydride equilibrium pressure increases due to the temperature rise from hydrogen absorption. This reduces the driving potential for mass transfer and corresponding slowdown of the absorption rate. Absorption is continued till the hydride equilibrium pressure becomes equal to the supply pressure (zero driving potential). It is also observed that the

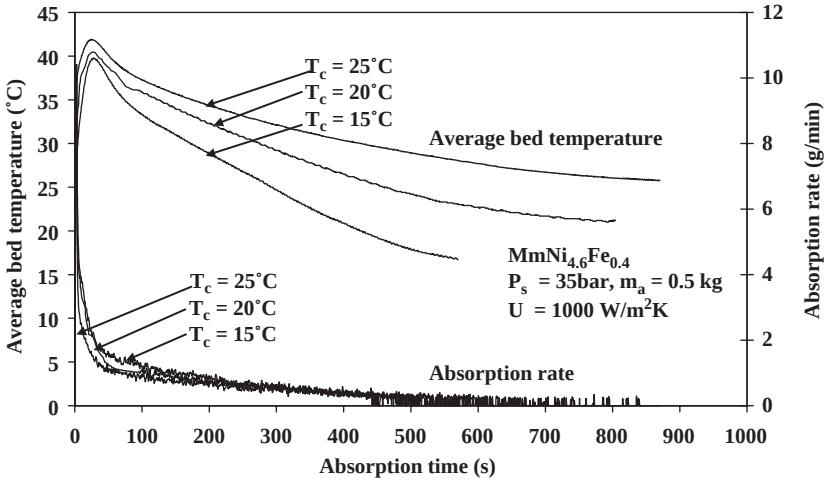

Fig. 9. Effect of cold fluid temperature on average bed temperature and hydrogen absorption rate for $MmNi_{4.6}Fe_{0.4}$.

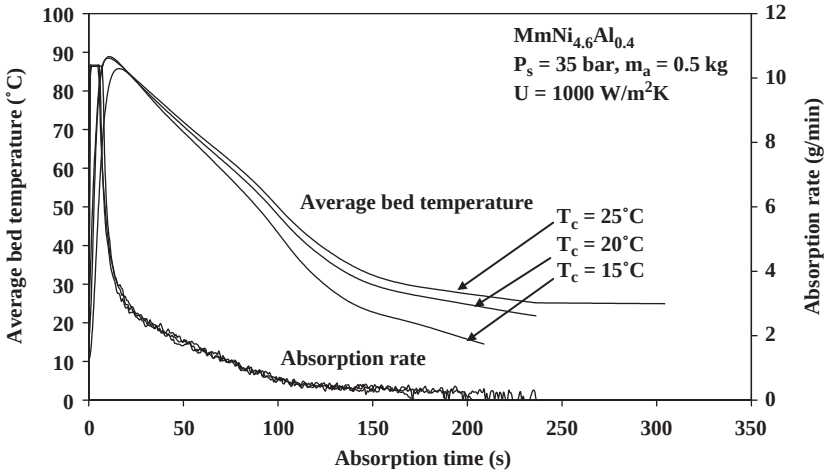

Fig. 10. Effect of cold fluid temperature on average bed temperature and hydrogen absorption rate for $MmNi_{4.6}Al_{0.4}$.

absorption rate increases with supply pressure. At higher supply pressures, the difference between supply pressure and hydride equilibrium pressure is more, which results in higher absorption rate and shorter cycle time. As the supply pressure decreases, the pressure difference also decreases leading to higher absorption time.

It is also observed from Figs. 5 and 6 that initially bed temperature increases sharply and then decreases gradually tending towards the preset value of the cold fluid temperature. Due to the poor thermal conductivity of the hydride bed, the generated heat of absorption is unable to be transferred from the bed to the cold fluid at the initial period of rapid absorption and hence the excess heat is stored in the hydride bed itself, resulting in a sudden rise in bed temperature. Later, bed temperature decreases gradually due to improved heat transfer due to higher temperature differential and fall in the rate of heat generation. The rise in bed temperature is higher at higher supply pressures due to faster kinetics.

It is also observed that for the given supply pressure, the rise in bed temperature during the initial stage of absorption for $MmNi_{4.6}Al_{0.4}$ is higher than that for $MmNi_{4.6}Fe_{0.4}$. This is due to the combined effects of a higher enthalpy of formation of the former (about 28.5 kJ/mol of H_2) and faster hydrogen absorption rate due to higher driving potential. Therefore, the rate of heat generation is higher, resulting in a sharper rise in bed temperature from 25 °C to about 90 °C.

Figs. 7 and 8 illustrate that the hydrogen storage capacities of $MmNi_{4.6}Fe_{0.4}$ and $MmNi_{4.6}Al_{0.4}$ increase with supply pressure. The increase is more rapid at lower supply

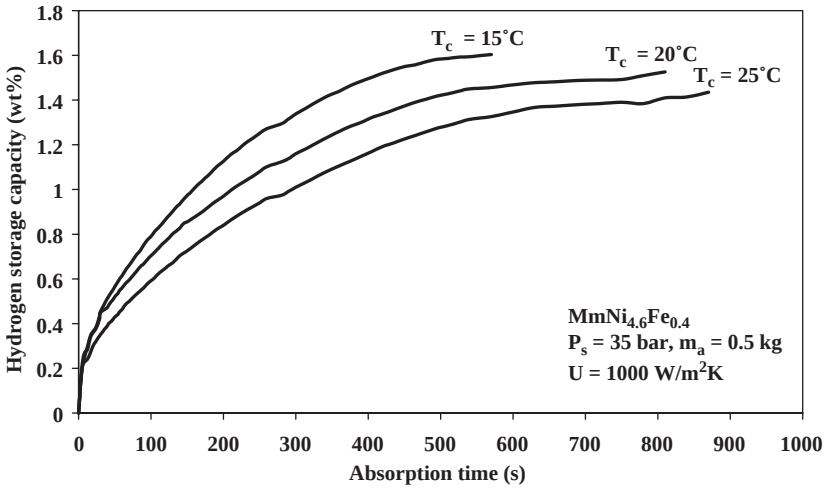

Fig. 11. Effect of cold fluid temperature on hydrogen storage capacity for $MmNi_{4.6}Fe_{0.4}$.

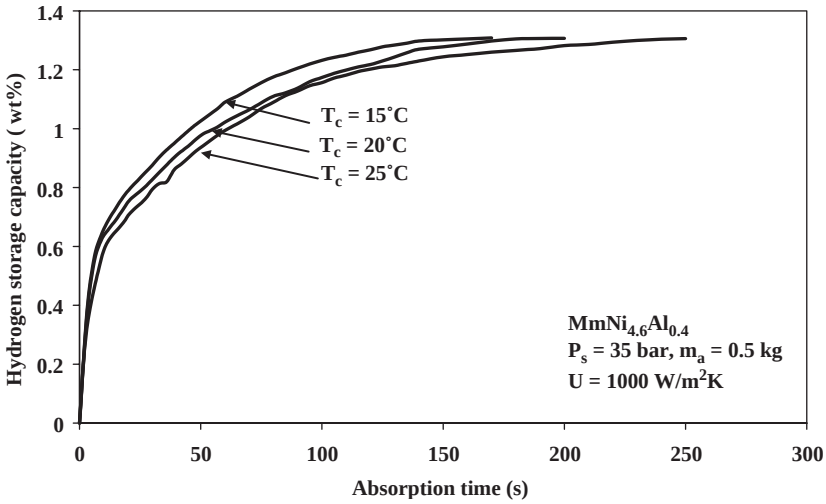

Fig. 12. Effect of cold fluid temperature on hydrogen storage capacity for $MmNi_{4.6}Al_{0.4}$.

pressures. Referring back to Figs. 5 and 6, higher supply pressures improve the absorption rate. For instance at 25 °C cold fluid temperature, it is seen from Fig. 4 that the equilibrium pressure at mid-plateau is about 25 bar for $MmNi_{4.6}Fe_{0.4}$ and 6 bar for $MmNi_{4.6}Al_{0.4}$. Absorption can take place up to about 35 and 25 bar, respectively, for $MmNi_{4.6}Fe_{0.4}$ and $MmNi_{4.6}Al_{0.4}$, beyond which there is no significant influence on absorption. Hence, the increase of supply pressures above 35 and 25 bar will not be beneficial for $MmNi_{4.6}Fe_{0.4}$ and $MmNi_{4.6}Al_{0.4}$, respectively. At conditions of 25 °C cold fluid temperature and 35 bar supply pressure, the maximum hydrogen storage capacity of 1.44 wt% is reached within 15 min of absorption for $MmNi_{4.6}Fe_{0.4}$, whereas 1.3 wt% is reached within 5 min of absorption for $MmNi_{4.6}Al_{0.4}$.

Figs. 7 and 8 also show that the hydrogen storage capacity (maximum hydrogen absorbed) increases with supply pressure for both the alloys. Referring back to Fig. 4, $MmNi_{4.6}Fe_{0.4}$ needs a minimum supply pressure of about 25 bar for hydrogen absorption, and $MmNi_{4.6}Al_{0.4}$ needs only about 5 bar at 25 °C. Further, $MmNi_{4.6}Fe_{0.4}$ gets saturated at a supply pressure of about 40 bar while $MmNi_{4.6}Al_{0.4}$ gets saturated at about 25 bar. The above observation goes well with the established properties of these two alloys. Both have sloped plateaus; $MmNi_{4.6}Fe_{0.4}$ starts from about 20 to 40 bar and $MmNi_{4.6}Al_{0.4}$ from 5 to 25 bar at 25 °C. As supply pressure is increased from 5 to 25 bar for $MmNi_{4.6}Al_{0.4}$, the maximum hydrogen absorption capacity also increases reaching the maximum

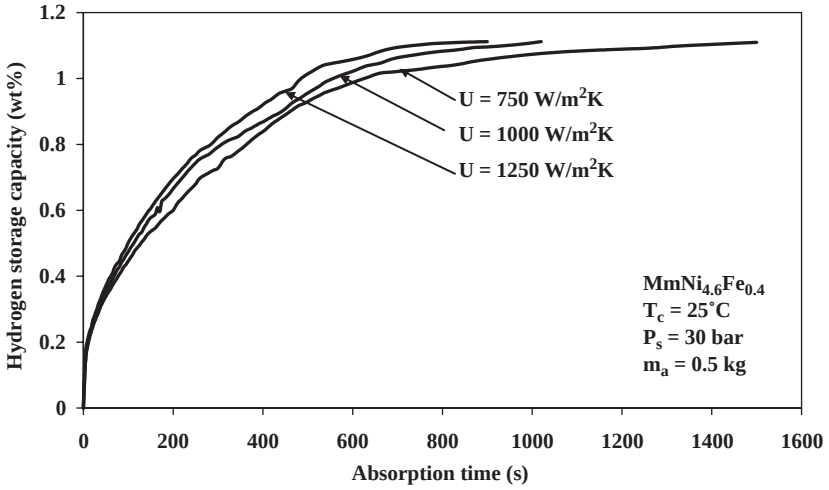

Fig. 13. Effect of overall heat transfer coefficient on hydrogen storage capacity for $MmNi_{4.6}Fe_{0.4}$.

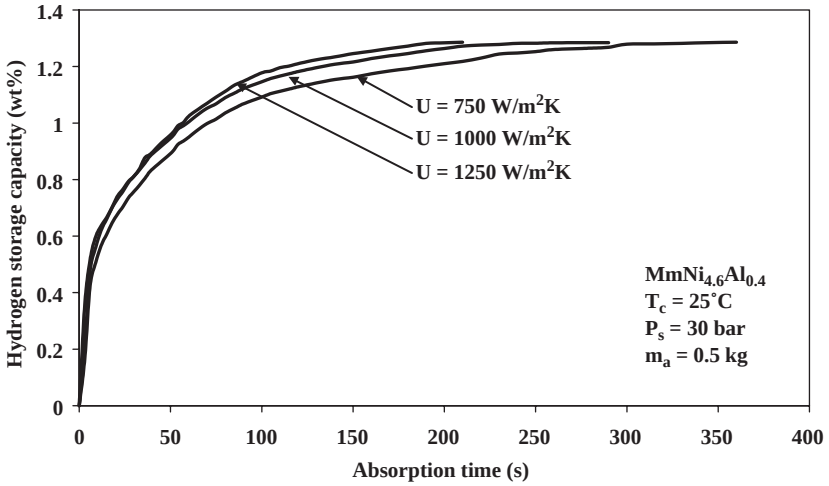

Fig. 14. Effect of overall heat transfer coefficient on hydrogen storage capacity for $MmNi_{4.6}Al_{0.4}$.

at 25 bar, beyond which the hydride equilibrium pressure increases rapidly with little increase in hydrogen storage capacity. $MmNi_{4.6}Fe_{0.4}$ also follows the same trend. Absorption time is also found to be lesser at higher supply pressures for both the alloys.

3.2. Effects of cold fluid temperature

The effects of cold fluid temperature on average bed temperature and the absorption rate illustrated in Figs. 9 and 10 show the expected trend that the hydrogen absorption rate is faster at lower cold fluid temperature ranges. At any given supply pressure, low cold fluid temperatures (and the accompanying low equilibrium pressure) cause an increase in the driving potential for mass transfer, resulting in higher absorption rate. However, in the case of $MmNi_{4.6}Al_{0.4}$, the effect of cold fluid temperature on absorption rate is not pronounced because the difference between supply and equilibrium pressures is large.

As illustrated in Fig. 11, the hydrogen storage capacity of $MmNi_{4.6}Fe_{0.4}$ increases with decrease in cold fluid temperature. At lower cold fluid temperatures, the hydride equilibrium pressure is low which results in a larger pressure difference between the supply pressure and the hydride equilibrium pressure. This results in an increase in the hydrogen absorption capacity. In order to reach the maximum hydrogen storage capacity, either supply pressure should be increased to above 35 bar by keeping the cold fluid temperature constant at 25 °C, or the cold fluid temperature should be decreased to below 15 °C by keeping the supply pressure

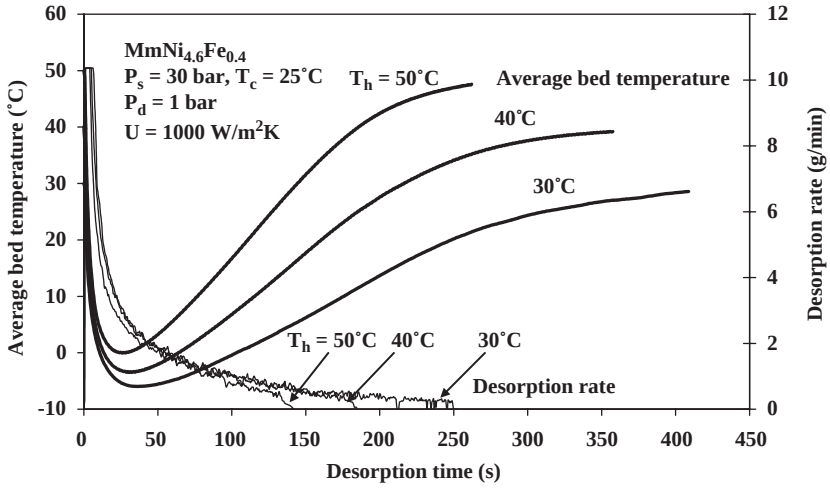

Fig. 15. Effect of hot fluid temperature on average bed temperature and hydrogen desorption rate for $MmNi_{4.6}Fe_{0.4}$.

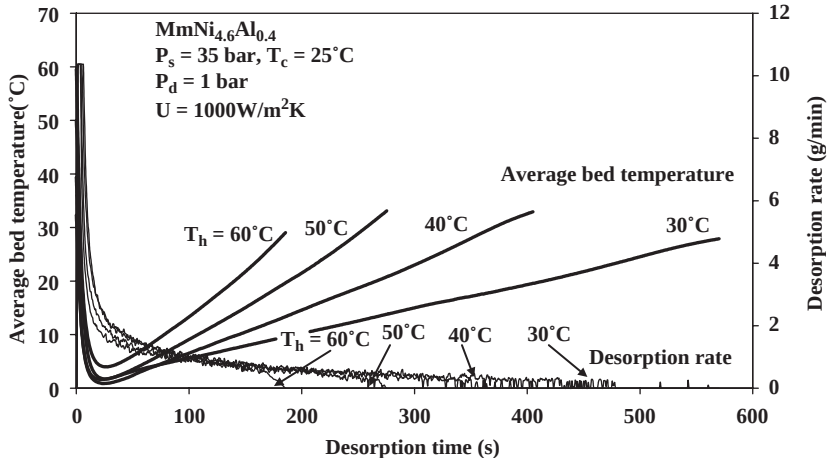

Fig. 16. Effect of hot fluid temperature on average bed temperature and hydrogen desorption rate for $MmNi_{4.6}Al_{0.4}$.

constant at 35 bar. Since absorption at temperatures below that of ambient necessitates additional cooling requirement, absorption may be carried out above 35 bar supply pressure as the industrial cylinders are loaded to above 100 bar storage pressure. The maximum storage capacity of 1.6 wt% is reached at 35 bar and 15 °C. In the case of $MmNi_{4.6}Al_{0.4}$, cold fluid temperature does not have any significant effect on hydrogen storage capacity for supply pressures of above 30 bar, which is illustrated in Fig. 12. However, it is expected that the hydrogen storage capacity increases with decrease in cold fluid temperature when the supply pressure is below 15 bar. Even though the mean plateau pressure at 25 °C is about 7 bar, due to high plateau slope, the hydride bed demands high supply pressure for completion of the absorption process. Hence, for any given supply pressure below 15 bar, lowering the cold fluid temperature below 25 °C would reduce the plateau pressure, resulting in an increase in the storage capacity. Since the cold fluid temperature below 25 °C generally necessitates a refrigeration system, absorption of hydrogen at supply pressures above 30 bar is preferred.

3.3. Effects of overall heat transfer coefficient

By definition, the overall heat transfer coefficient combines the effects of convective resistance offered by the heat transfer fluid to the reactor wall and the conductive resistance offered by the reactor wall. The contact resistance between the reactor wall and the hydride particle is neglected. Since the conductive resistance is fixed, the overall heat transfer coefficient can be varied by changing the flow rate of the heat transfer fluid. Figs. 13 and 14 together show that the overall heat transfer coefficient does not have any

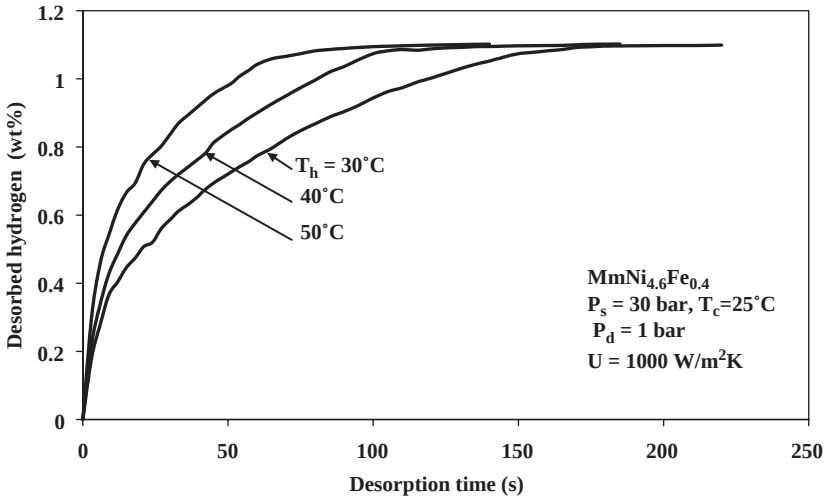

Fig. 17. Effect of hot fluid temperature on desorbed hydrogen for $MmNi_{4.6}Fe_{0.4}$.

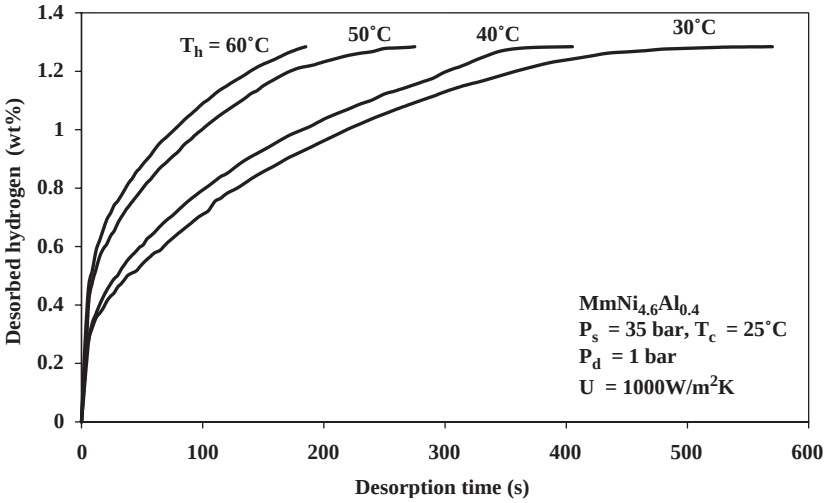

Fig. 18. Effect of hot fluid temperature on desorbed hydrogen for $MmNi_{4.6}Al_{0.4}$.

significant effect on hydrogen storage capacity. However, higher overall heat transfer coefficient reduces the absorption time by facilitating faster removal of the absorption heat from the bed. Hence, higher fluid flow rates are preferred, especially at high supply pressures.

3.4. Desorption characteristics

The desorption characteristics of $MmNi_{4.6}Fe_{0.4}$ and $MmNi_{4.6}Al_{0.4}$ shown in Figs. 15 and 16 reveal that the desorption rates are improved at higher hot fluid temperatures due to higher mass transfer driving potential. For $MmNi_{4.6}Fe_{0.4}$, the bed temperature initially drops steeply down to about −7 °C and then increases gradually reaching the preset value of the hot fluid temperature. Due to poor thermal conductivity of the hydride bed, the necessary amount of heat is not being transferred to the bed at the initial stage of rapid desorption, and hence the hydride bed is taking the heat of desorption from the bed itself, resulting in a sudden fall in temperature. In addition, the equilibrium temperature at 1 bar is below 0 °C and therefore desorption at 1 bar pressure also helps to bring down the bed temperature. Desorption characteristics of $MmNi_{4.6}Al_{0.4}$ also follow a similar trend of $MmNi_{4.6}Fe_{0.4}$. Figs. 17 and 18 show that most of the hydrogen in $MmNi_{4.6}Fe_{0.4}$ is desorbed within the initial 75 s, while $MmNi_{4.6}Al_{0.4}$ takes

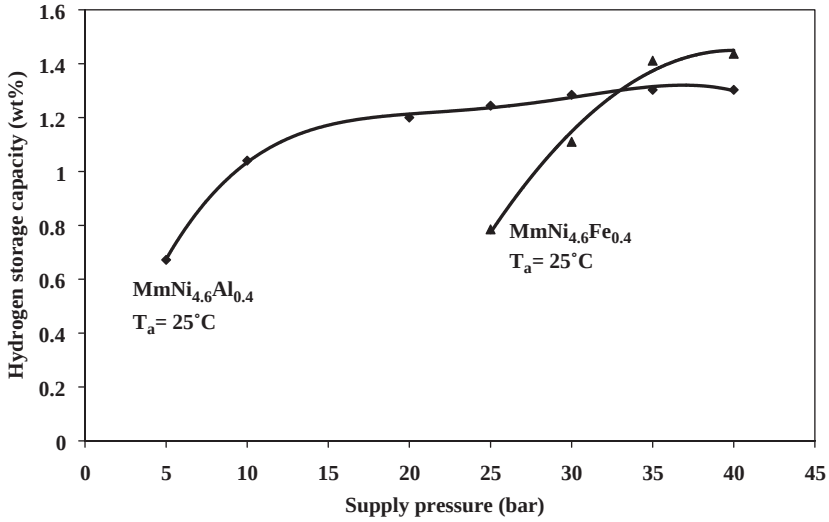

Fig. 19. Variation of hydrogen storage capacities with supply pressure.

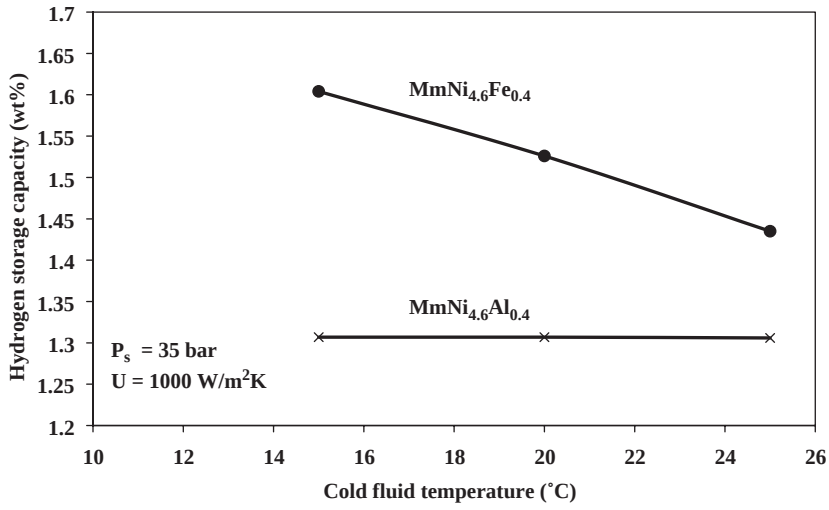

Fig. 20. Variation of hydrogen storage capacities with cold fluid temperature.

nearly about 250 s at a hot fluid temperature of 50 °C. This is due to higher equilibrium pressure of the former, which corresponds to higher mass transfer driving potential.

Figs. 19 and 20 make a further comparison of the two alloys. $MmNi_{4.6}Fe_{0.4}$ and $MmNi_{4.6}Al_{0.4}$ store about 1.44 and 1.3 wt% at the supply conditions of 35 bar and 25 °C, respectively. The maximum storage capacity of a former increases further to 1.6 wt% if the cold fluid temperature is reduced down to 15 °C. It is also observed that supply pressure has a significant effect on the hydrogen storage capacity of both the alloys. Referring to Fig. 20, the effect of cold fluid temperature on the hydrogen storage capacity of $MmNi_{4.6}Al_{0.4}$ is negligible when supply pressure is increased to above 35 bar. However, with reference to Fig. 4, the effect of cold fluid is significant for supply pressures below 15 bar.

4. Conclusions

Two mischmetal-based alloys are tested in a metal hydride storage device at various operating conditions. At any given cold fluid temperature, the hydrogen storage capacity increases with supply pressure for both the alloys. In addition to higher storage capacity, the absorption time was also found to be lesser at higher supply pressures for both the alloys. However, at 25 °C, increase of supply pressures above

35 bar for $MmNi_{4.6}Fe_{0.4}$ and 25 bar for $MmNi_{4.6}Al_{0.4}$ does not have any significant effect on hydrogen storage capacity. Cold fluid temperature has a strong influence on hydrogen storage capacity at supply pressures below 30 and 15 bar for $MmNi_{4.6}Fe_{0.4}$ and $MmNi_{4.6}Al_{0.4}$ alloys, respectively. The former stores about 1.6 wt%, while the latter stores about 1.3 wt% at a supply pressure of 35 bar and an absorption temperature of 15 °C. The effect of overall heat transfer coefficient on hydrogen storage capacity is negligible for both the alloys. However, higher overall heat transfer coefficients are preferred when the supply pressure is above 30 bar for accomplishing fast removal of absorption heat. Desorption characteristics of both the alloys are found to be faster at higher hot fluid temperatures. $MmNi_{4.6}Fe_{0.4}$ takes about 75 s and $MmNi_{4.6}Al_{0.4}$ takes about 250 s for completing desorption at 50 °C.

Acknowledgements

The authors thank the Ministry of Non-conventional Energy Sources (MNES), Government of India, for their financial support. The authors also express their sincere thanks to Prof. O.N. Srivastava, Banaras Hindu University, for supplying the alloys.

References

[1] Sinha VK, Wallace WE. $Zr_{0.7}Ti_{0.3}Mn_2Fe_{0.8}$ as a material for hydrogen storage. J Less-Common Metals 1982;87:297–303.
[2] Sinha VK, Wallace WE. Hydrides of $ZrMn_2$ based alloys substoichiometric in zirconium for engineering applications. J Less-Common Metals 1985;106:199–210.
[3] Sinha VK, Yu GY, Wallace WE. Hydrogen storage in some ternary and quaternary zirconium based alloys with the C14. J Less-Common Metals 1985;106:67–77.
[4] Topler J, Feucht K. Results of a test fleet with metal hydride motorcars, Presented as an invited lecturer at the international symposium on Metal—Hydrogen systems, fundamentals and applications. Stuttgart, FRG: September 4–9, 1989.
[5] Hagstrom MT, Lund PD, Vanhanen JP. Metal hydride hydrogen storage for near-ambient temperature and atmospheric pressure applications a PDSC STUDY. Int J Hydrogen Energy 1995;20(11):897–909.
[6] Singh BK, Singh AK, Srivastava ON. Improved hydrogen sorption characteristics in $FeTi_{1+x}Mm$ material. Int J Hydrogen Energy 1996;21(2):111–7.
[7] Davidson DJ, Srivastava ON. Studies on the hydrogen absorption/desorption properties of $Zr_{1-x}Mm_xFe_{1.4}Cr_{0.6}$ and $Zr_{1-2x}Mm_xTi_xFe_{1.4}Cr_{0.6}$ ($x = 0,0.05,0.1$ and 0.2) Laves phase alloys. Int J Hydrogen Energy 2001;26:219–23.
[8] Du YL, Yahg XG, Lei YQ, Zhang MS. Hydrogen storage properties of $Zr_{0.8}Ti_{0.2}$ $(Ni_{0.6}Mn_{0.3-x}V_{0.1+x}Cr_{0.05})_2$ ($x = 0.0,0.05,0.15,0.15,0.2$) alloys. Int J Hydrogen Energy 2002;27:695–7.
[9] Sitaram V, Mani N, Kesavan TR, Ramaprabhu S. Hydrogen storage studies in $Zr_{0.9}Ho_{0.1}MnFe_{0.5}Co_{0.5}$ and $Zr_{0.9}Ho_{0.1}MnFe_{0.5}Ni_{0.5}$. Int J Hydrogen Energy 2002;27:413–8.
[10] Singh RK, Gupta BK, Lototsky MV, Srivastava ON. On the synthesis and hydrogenation behavior of $MmNi_{5-x}Fe_x$ alloys and computer simulation of their P–C–T curves. J Alloys Compounds 2004;373(1–2):208–13.
[11] Muthukumar P, Kevin Abraham, Rajendra Prasad UA, Prakash Maiya M, Srinivasa Murthy S. Screening of metal hydrides for engineering applications. 16th International Conference on Efficiency, Costs, Optimization, Simulation and Environmental Impact of Energy Systems. Copenhagen, Denmark: June 30–July 2, 2003.